

# Reed Leaf-Inspired Graphene Films with Anisotropic Superhydrophobicity

Hao-Bo Jiang,<sup>†,‡</sup> Yu-Qing Liu,<sup>†</sup> Yong-Lai Zhang,<sup>\*,†,Ⓞ</sup> Yan Liu,<sup>‡</sup> Xiu-Yan Fu,<sup>†</sup> Dong-Dong Han,<sup>†</sup> Yun-Yun Song,<sup>‡</sup> Luquan Ren,<sup>‡</sup> and Hong-Bo Sun<sup>\*,§</sup>

<sup>†</sup>State Key Laboratory of Integrated Optoelectronics, College of Electronic Science and Engineering, Jilin University, 2699 Qianjin Street, Changchun 130012, China

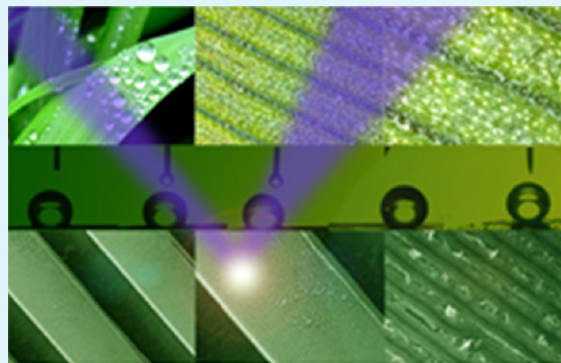
<sup>‡</sup>Key Laboratory of Bionic Engineering (Ministry of Education), Jilin University, Changchun 130022, China

<sup>§</sup>State Key Lab of Precision Measurement and Instruments, Department of Precision Instrument, Tsinghua University, Beijing 100084, China

## Supporting Information

**ABSTRACT:** Controlling the wettability of graphene and its derivatives is critical for broader applications. However, the dynamic dewetting performance of graphene is usually overlooked. Currently, superhydrophobic graphene with an anisotropic wettability is rare. Inspired by natural reed leaves, we report an ingenious fabrication process combining photolithography and laser holography technologies to create biomimetic graphene surfaces that demonstrate anisotropic wettability along two directions of grooved hierarchical structures, which are similar to reed leaf veins. Microgrooved structures with a period of 200  $\mu\text{m}$  were fabricated via photolithography to endow the substrate with an obvious anisotropic wettability. Two-beam laser interference treatments of the graphene oxide (GO) film on the grooved substrate removed most of the hydrophilic oxygen-containing groups on the GO sheets and increased the surface roughness by introducing additional hierarchical micro–nanostructures. The combined effects endowed the resultant graphene films with a unique anisotropic superhydrophobicity similar to that of reed leaves. Superhydrophobic graphene surfaces with anisotropic antiwetting behavior might allow further innovations based on graphene in the fields of bionics and electronics.

**KEYWORDS:** *bioinspired graphene, graphene oxide, photolithography, laser holography technology, anisotropic superhydrophobicity*



## INTRODUCTION

Natural creations possess well-designed physiological structures and amazing functionalities, and these properties continuously inspire scientists and engineers in multidisciplinary fields to develop artificial materials that feature similar or better properties.<sup>1,2</sup> For instance, nacre demonstrates a high mechanical strength due to the well-assembled brick-and-mortar architecture of inorganic calcium carbonate and biomacromolecules.<sup>3</sup> Butterfly wings and peacock feathers show both brilliant structural colors and superhydrophobicity due to the presence of multiscale photonic structures.<sup>4,5</sup> Insect compound eyes are natural optical devices with unique antireflection and antifogging properties due to their multiscale surface structures that consist of closely packed micro-ommatidia arrays.<sup>6</sup> Among bionic studies, the unique dewetting properties of solid surfaces have attracted interest since wettability control is important in a wide range of scientific fields, e.g., biomedical devices and tissue engineering.<sup>7,8</sup> In nature, several distinct, antiwetting structures exist. Typically, lotus leaves show Cassie state superhydrophobicity, i.e., water droplets easily roll off the surface.<sup>9</sup> In contrast, rose petals

demonstrate Wenzel's model hydrophilicity and a water droplet can be firmly pinned to the surface.<sup>10</sup> In addition, *Nepenthes* pitcher plants introduce a new paradigm for slippery wettability due to their lubricant-infused surfaces.<sup>11</sup> Rice and reed leaves exhibit anisotropic wettability, i.e., water droplets prefer to roll along the direction parallel to the rice leaf edge rather than the perpendicular direction.<sup>12</sup> Motivated by the potential impact of such dewetting surfaces on fundamental science and practical applications, a wide variety of materials with special surface wettability, ranging from metal/metal oxides<sup>13,14</sup> to polymers,<sup>15</sup> carbon materials,<sup>16</sup> and biomaterials,<sup>17</sup> have been extensively studied both theoretically and experimentally. Currently, although rapid progress has been achieved in this dynamic field, efforts have mainly been devoted to developing new antiwetting materials because the combination of a special surface wettability and a novel material leads to exceptional

Received: March 6, 2018

Accepted: May 3, 2018

Published: May 3, 2018

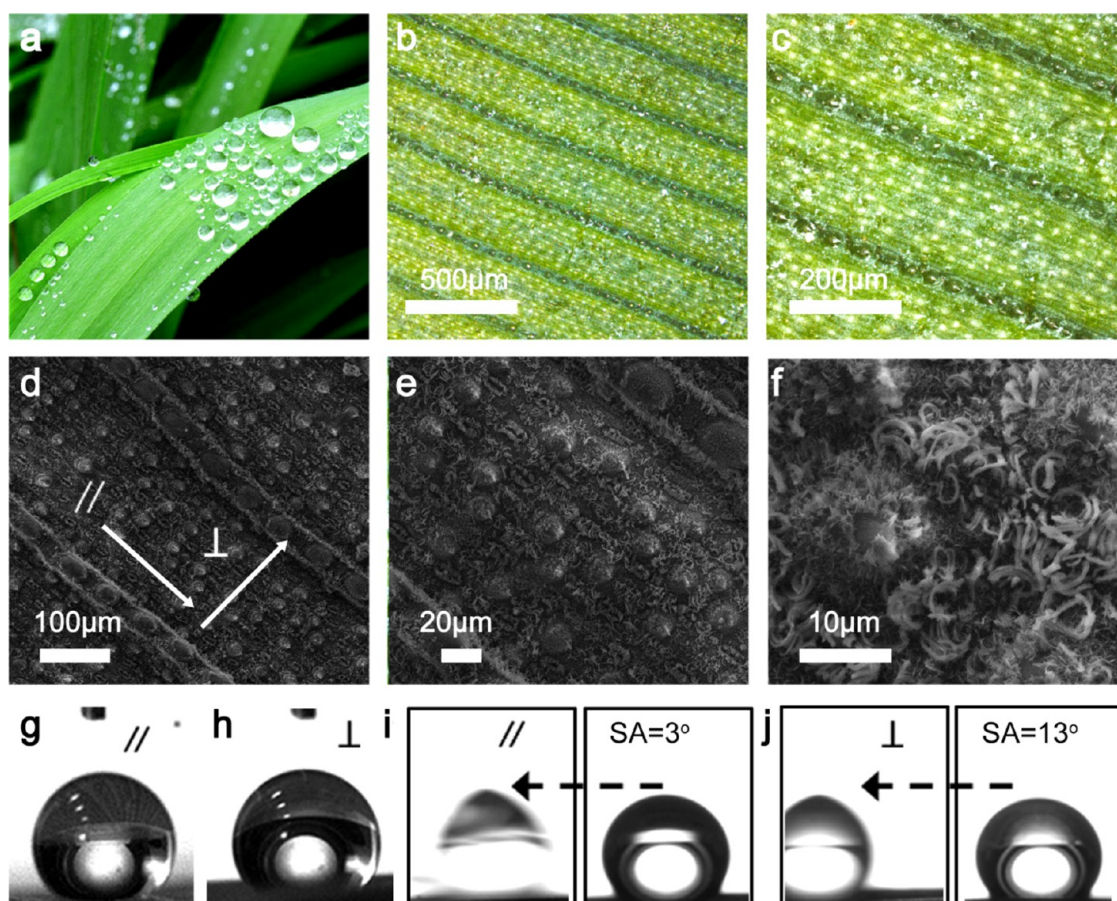


**Figure 1.** Surface morphology and wettability of natural reed leaves. (a) Photograph of a reed leaf. (b, c) CLSM images of the surfaces of reed leaves. (d–f) SEM images of the surfaces of reed leaves. (g, h) Photographs of a water droplet on a reed leaf surface; the CAs were measured along the parallel and perpendicular directions. (i, j) Photographs of the SAs measured along the parallel and perpendicular directions.

innovations that contribute to the development of multifunctional biomimetic devices.

Graphene is a unique, two-dimensional carbon material with excellent properties,<sup>18,19</sup> e.g., ultrahigh carrier mobility,<sup>20</sup> good electrical conductivity,<sup>21</sup> high transmittance,<sup>22</sup> and biocompatibility,<sup>23</sup> and because of these properties, graphene has become prominent in material science. Because of its outstanding physical/chemical properties, graphene is promising for potential applications in electronic devices,<sup>24,25</sup> optical devices,<sup>26</sup> biochips,<sup>27</sup> and intelligent robots.<sup>28</sup> Therefore, sophisticated control over the surface wettability of graphene and its derivatives has attracted attention. The wettability of a solid surface is dominated by both the surface chemical composition (surface energy) and the topological structures.<sup>12,29</sup> On the basis of this basic principle, graphene surfaces with a special wettability have been successfully fabricated via different approaches. For instance, Zang et al. prepared superhydrophobic graphene surfaces with well-controlled one-direction and two-direction wrinkle structures by first transferring chemical vapor deposition (CVD)-grown, few-layer graphene onto a stretched elastic substrate and then releasing the substrate.<sup>30</sup> Additionally, structured copper or nickel templates, e.g., foamed nickel and laser-structured copper film, have also been employed to create superhydrophobic graphene surfaces via a template-directed CVD method.<sup>31,32</sup> The development of superhydrophobic graphene is not limited to CVD methods. Graphene oxides (GOs) that permit tractable solution processing are considered ideal alternatives to create

superhydrophobic graphene surfaces since rough structure fabrication and low-surface-energy material functionalization are easier with GO than with pristine graphene.<sup>33</sup> Typical strategies, such as covalent grafting of hydrophobic groups,<sup>34</sup> solvent modification,<sup>35</sup> freeze-drying methods,<sup>36</sup> and laser processing,<sup>16</sup> have been employed to create superhydrophobic graphene using GO as a raw material. However, the majority of previous works on superhydrophobic graphene is based on disordered, rough graphene surfaces and the superhydrophobicity is limited to Wenzel's state. Although the static contact angles (CAs) of these graphene surfaces are greater than  $150^\circ$ , i.e., superhydrophobic, the dynamic dewetting performance is usually overlooked. Currently, Cassie state superhydrophobic graphene with self-cleaning properties is rare and precise control of the anisotropic antiwetting behavior through a biomimetic mechanism has not been achieved. A possible reason for this is that graphene is a single-atom-thick, two-dimensional material, and considerable difficulties might arise in molding the ultrathin surface into hierarchical micro-nanostructures like those present in nature.

In this paper, we report a reed leaf-inspired biomimetic fabrication of superhydrophobic graphene surfaces with anisotropic antiwetting behavior using a combination of photolithography and laser holography techniques. Hierarchically structured graphene films with large periodic grooves (200  $\mu\text{m}$  periods), microgratings (2  $\mu\text{m}$  periods), and layered nanostructures (10–100 nm interlayer spacings) were fabricated by first coating GO on a grooved SU-8 substrate

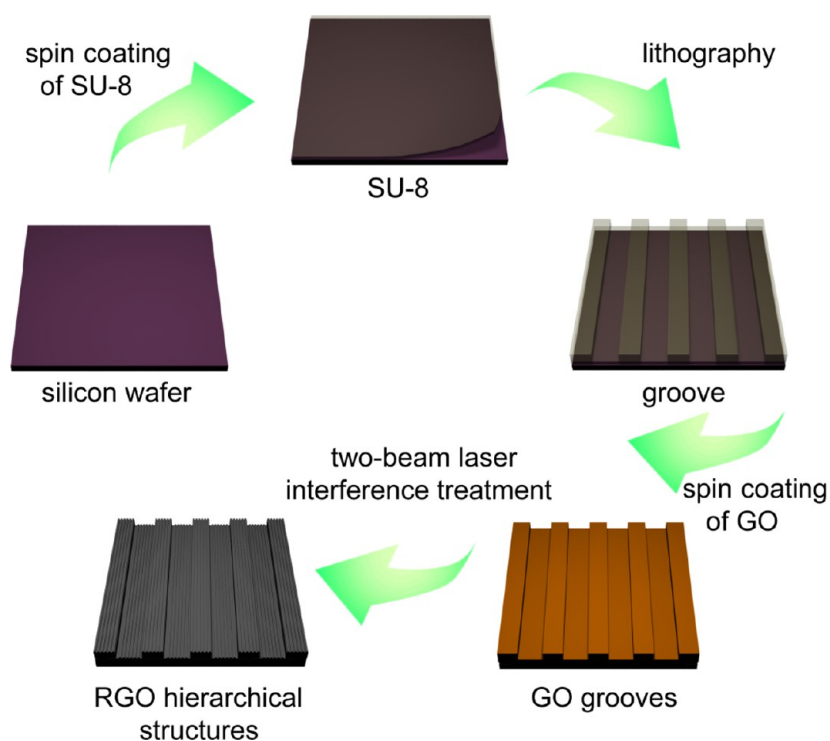


**Figure 2.** Schematic illustration of the fabrication process for biomimetic graphene surfaces.

and then subjecting the GO coating to a laser holography treatment. The combined effects of constructing such hierarchical structures and modulating the surface energy via laser treatment endow the resultant graphene films with unique anisotropic superhydrophobicity. To the best of our knowledge, biomimetic graphene surfaces with antiwetting properties similar to those of reed leaves have not been reported. Achieving better control over the dewetting properties of graphene is very important for furthering graphene applications. For instance, graphene and GO have been proven biocompatible scaffolds for human mesenchymal stem cells. Thus, superhydrophobic graphene surfaces with an anisotropic antiwetting behavior may be potentially important in multidisciplinary fields, such as microfluidics and tissue engineering.

## EXPERIMENTAL METHODS

**Materials and Fabrication Technology.** First, the Si wafer substrates were cleaned with acetone, absolute ethanol, and deionized water in sequence. Then, the SU-8 photoresist diluted with cyclopentanone was spin-coated onto the Si wafer substrates and dried at 95 °C in a baking oven for 2 h to remove the cyclopentanone solvent. Here, the epoxy negative resin SU-8 2025 was purchased from Nano MicroChem Company. The thickness of coated SU-8 layer has been tested with the ratio of the SU-8 photoresist, cyclopentanone, and the speed of coating. A periodic stripe pattern mask plate was used to cover the baked samples, which were exposed to an ultraviolet light source. After lithography, the patterned samples were heated again to sharpen the structures of the pattern. Developer was used in the last step to completely expose the patterned structures. GO was prepared from purified natural graphite (Aldrich, <150 μm) by following Hummers' method. The as-synthesized GO was dispersed into individual sheets in distilled water at a concentration of 3 mg/mL with the aid of ultrasound. The GO was spin-coated onto the SU-8 substrates and dried at room temperature. Then, a frequency-tripled, Q-switched, single-mode Nd:YAG laser (Spectra-Physics) with an approximately 10 ns pulse width ( $\lambda = 355$  nm; beam size, ca. 8 mm in diameter) was split into two beams with the same optical path lengths

to the sample. The biomimetic graphene surfaces with multilevel structures were fabricated by exposing the samples to the interfered laser region. Taking advantage of laser holography technique, the periodicity of the grating could be precisely controlled by changing the angle of two laser beams, as shown in the following equation

$$\Lambda = \frac{\lambda_F}{2 \sin(\theta/2)}$$

where  $\Lambda$  is the period,  $\lambda_F$  is the laser wavelength, and  $\theta$  is the angle between the two beams.

**Characterization.** Scanning electron microscopy (SEM) images were obtained using a field emission scanning electron microscope (JSM-7500F, JEOL, Japan). Confocal laser scanning microscopy (CLSM, OLS4100, Japan) was utilized to measure the surface morphologies of the samples. Atomic force microscopy (AFM) images were obtained using a NanoWizard II BioAFM instrument (JPK Instruments AG, Berlin, Germany) in the tapping mode. X-ray photoelectron spectroscopy (XPS) was performed using an ESCALAB 250 spectrometer. The CA measurements were taken using the Contact Angle System OCA 20 (DataPhysics Instruments GmbH, Germany) at ambient temperature. The CAs were measured using a 5 μL water droplet.

## RESULTS AND DISCUSSION

**Anisotropic Wettability of Reed Leaves.** Reeds grow in ponds, rivers, and streams. To provide adequate moisture to the root segment, the surfaces of reed leaves have special structural patterns that guide dew drops to roll in the direction of the root. To obtain better insight into the wettability of reed leaves, the surface topography of fresh reed leaves must first be characterized. As shown in Figure 1, reed leaves demonstrate superhydrophobicity and dew drops can maintain a sphere shape on the surface of reed leaves. Using confocal laser scanning microscopy (CLSM), we observed ordered, groove-like microstructures with a period of 200–400 μm (Figure 1b). The high-resolution CLSM image (Figure 1c) and scanning electron microscopy (SEM) images (Figure 1d–f) show small,

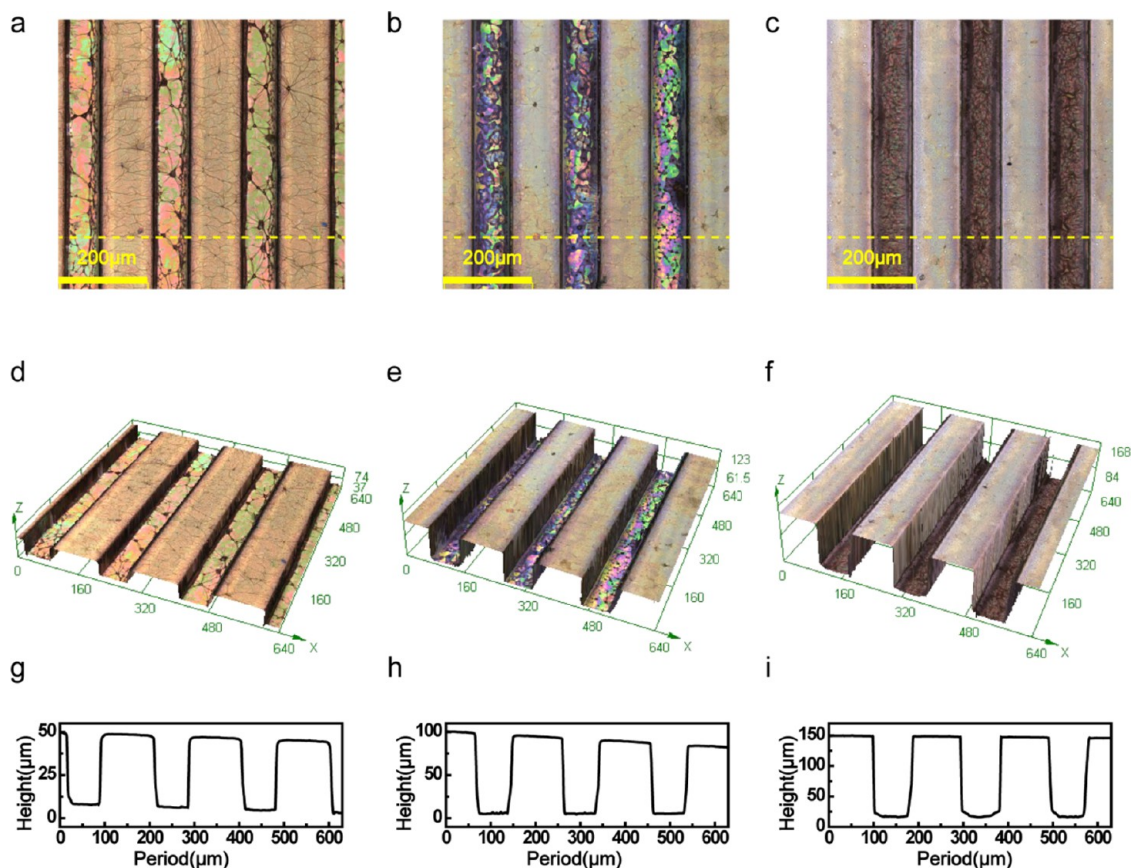


**Figure 3.** CLSM images of the grooved structures with different groove depths: (a) 50  $\mu\text{m}$ , (b) 100  $\mu\text{m}$ , and (c) 150  $\mu\text{m}$ . (d–f) Three-dimensional-transformed CLSM images of the grooved structures with heights of 50, 100, and 150  $\mu\text{m}$ , respectively. (g–i) Height profiles of the surface along the yellow dashed lines in (a), (b), and (c), respectively.

periodic grating structures and a parallel arrangement of micropapillae with a period of ca. 10–20  $\mu\text{m}$ . Interestingly, the micropapillae distribute in one line, which is parallel to the direction of the large periodic grooves. Additionally, some spiral nanostructures exist around the micropapillae. The presence of these composite and hierarchical structures is the reason for the unique surface wettability and anisotropic superhydrophobicity. To test the anisotropic wettability of the reed leaves, the static water CAs and sliding angles (SAs) in two directions, which were defined as the perpendicular and parallel directions with respect to the groove direction, were measured (Figure 1g,h). Because of the multilevel structures on the surface of the reed leaves, the CA of the reed leaf surface reached superhydrophobic values. The CA value along the parallel direction was  $\sim 154^\circ$ , which is  $3^\circ$  larger than that along the vertical direction ( $151^\circ$ ). For comparison, we also tested the SAs along the two directions, as shown in Figure 1i,j. In this case, the anisotropic superhydrophobicity was obvious. The SA along the parallel direction was approximately  $3^\circ$ , which was much smaller than the SA along the vertical direction ( $13^\circ$ ). On the basis of these characterization results, we concluded that the reed leaf surfaces show obvious anisotropic wettability in two directions along the large periodic grooves. Because the wettability phenomena of solid surfaces are generally associated with surface roughness, the apparent anisotropic, superhydrophobic wettability of reed leaves is due to their special surface structures.

**Fabrication of Biomimetic Graphene Surfaces.** Inspired by the multilevel structures of reed leaves, we fabricated

hierarchically structured graphene surfaces with anisotropic wettability through a combination of photolithography and laser holography technologies. A sketch of the fabrication process is shown in Figure 2. First, we used photolithography technology to construct the groove structures on a smooth Si wafer using a conventional photopolymer, SU-8. We chose SU-8 as substrate material since it is tractable for patterning through simple lithography. In fact, SU-8 is not the only choice for fabricating hierarchically structured graphene surfaces. Other functional materials that can be processed into similar patterns, for instance, poly(dimethylsiloxane) (PDMS), are also workable (Figure S5). The as-formed groove structure with a period of 200  $\mu\text{m}$  can provide a structured gradient substrate to create a surface with anisotropic wettability. Second, GO was spin-coated onto the surface of the SU-8 grooves. Since aqueous GO solutions feature good solution-processing properties, a continuous GO film formed on the grooved surface. To endow the grooved GO surface with additional micro–nanostructures, we performed a two-beam laser interference treatment to reduce the GO. The maximum light spot for the fabrication of the grating structure is about 1 cm in diameter (Figure S7), and it takes about 30 s to fabricate each spot. In this case, large area of superhydrophobic graphene surface can be prepared by splicing each spot together. Both the surface structures and chemical composition govern the surface wettability. The laser interference can create hierarchical micro–nanostructures, which significantly increase the surface roughness, and alter the surface chemical composition by removing hydrophilic oxygen-containing groups (OCGs). The

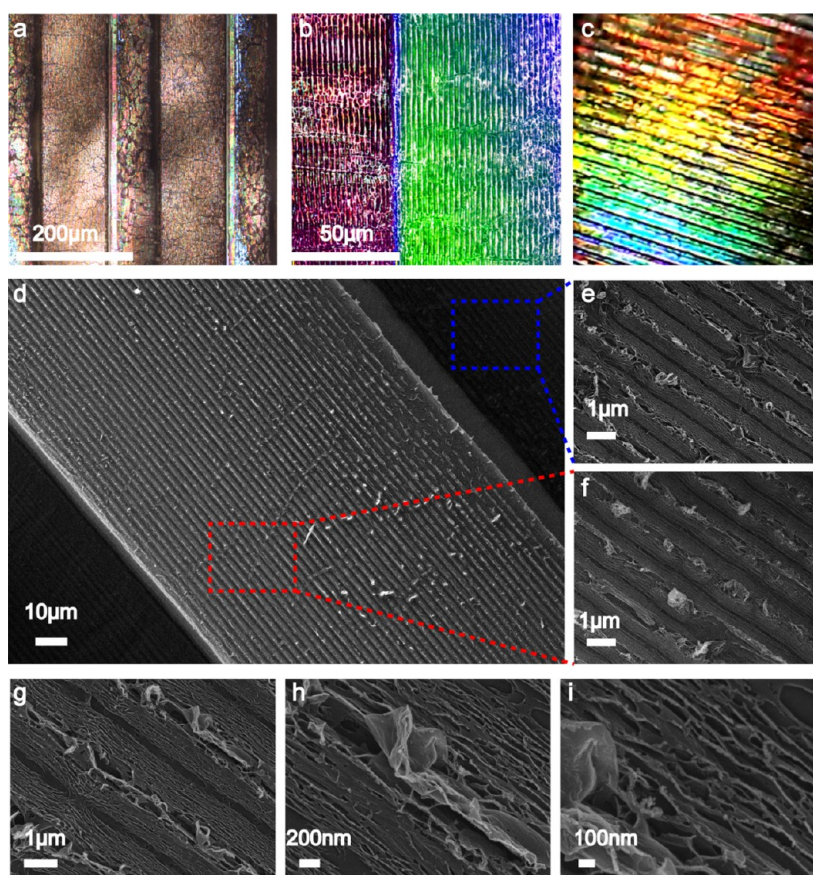


**Figure 4.** (a, b) CLSM images of the biomimetic graphene surface. (c) Photograph of the structural color of the biomimetic graphene surface. (d–i) SEM images of the biomimetic graphene surfaces. (e, f) SEM images of the bottom and top regions, respectively. (g–i) SEM images of the detailed micro–nanostructures.

combined effect of hierarchical structuring and GO photo-reduction endows the resultant graphene film with anisotropic and superhydrophobic wettability.

In this study, we fixed the period of the grooves at  $200\ \mu\text{m}$  and both the top and gap of the grooves were  $100\ \mu\text{m}$ . To optimize the depth of the grooves, we prepared three typical structures with depths of 50, 100, and  $150\ \mu\text{m}$ . To coat the hydrophobic SU-8 surface with hydrophilic GO, the grooved SU-8 surface has to be treated by  $\text{O}_2$  plasma (Figure S9), after which the surface becomes hydrophilic. By coating a GO layer on the surface of the grooved structure, the substrates maintained a structure similar to that without GO since the thickness of the GO layer was much smaller than the depth of the grooves. The thickness of the GO films is  $\sim 1.4\ \mu\text{m}$  according to the AFM image of the GO film (Figure S3). Figure 3 shows the CLSM images of the grooved structures with a GO layer. The images in Figure 3a–c show a continuous GO layer on the top and bottom of the grooves. The coatings of SU-8 and GO were pretty smooth (Figure S8). Some small iridescent patches were observed at the bottom of the grooves in the GO-grooved structures, indicating stacking of the GO sheets. The three-dimensional (3D)-transformed CLSM images of the GO-groove patterns show a visual observation of the surface topography and fluctuations (Figure 3d,e). The height profiles along the yellow line in the images in Figure 3a–c confirmed the period and height of the GO-grooved structures (Figure 3g–i).

In addition to the large grooved structures with a tunable depth, we also fabricated additional hierarchical micro–

nanostructures on the GO surfaces to mimic the multilevel structure of reed leaves. To better control the surface wettability, the surface chemical composition should also be considered. The laser holography technique is a powerful tool for rapid, mask-free, large-area micro–nanofabrication. In this study, laser holography was used to create biomimetic micro–nanostructures on the GO films through the synergetic effect of photoreduction and laser structuring of GO. Briefly, in the laser interference region, the laser intensity distribution is constant along the  $y$ -axis and sinusoidal along the  $x$ -axis. The highest laser intensity is calculated to be 4 times of each laser beam, and the minimum value is 0. In the high-laser-intensity region, the OCGs were thoroughly removed, whereas in the low-intensity region, the GO survived and was reduced partially. As previously mentioned, the small, periodic grating structures on the surface of reed leaves are parallel to the large periodic grooves. To imitate the hierarchical structures of reed leaves, we fabricated microscale grating structures along the large groove via laser holography. Figure 4a shows the CLSM image of the biomimetic graphene surface. After the laser ablation, a grating structure formed on the surface of the large GO-grooved structures. The magnified CLSM image (Figure 4b) clearly shows ordered grating structures that are parallel to the boundary of the grooves. Interestingly, the formation of the grating structure accounts for the brilliant rainbow color observed on the surface of the samples (Figure 4c). Because of the scattering and diffraction of the grating-like structures, our graphene films with hierarchical microstructures show iridescence. The SEM image shows that the small grating

structures were symmetrically distributed on the top and bottom of the grooved structure (Figure 4d). Moreover, the grating structures on the bottom of the grooved structure were similar to those on the top area (Figure 4e,f). The period of the grating structure was  $2\ \mu\text{m}$ . Figure 4g–i shows the magnified SEM images of the graphene grating structures. A nanoscale roughness was observed on the surface of the grating structures. The formation of these hierarchical micro–nanostructures is essential for achieving a superhydrophobic surface.

**Characterization of Biomimetic Graphene Surfaces.** In addition to characterizing the grating structures by CLSM and SEM, the heights of the grating structures were evaluated by high-resolution CLSM and atomic force microscopy (AFM). Figure 5a shows that the grating structures were uniform over a

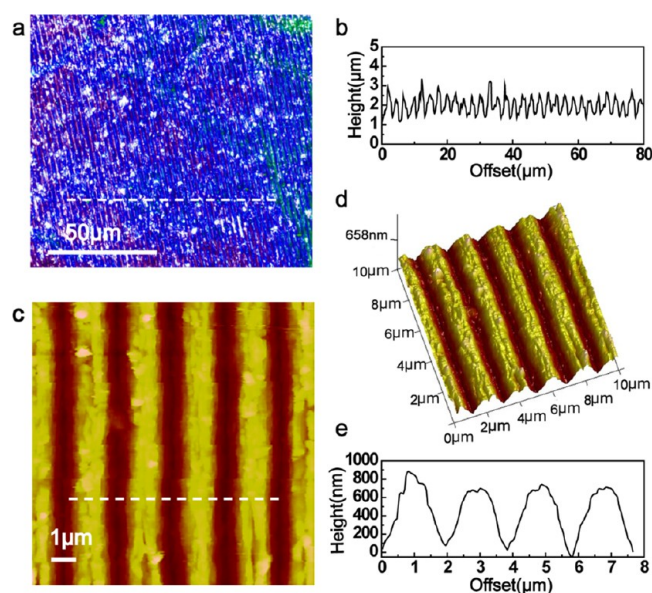


**Figure 5.** (a) CLSM image of the grating structures on the biomimetic graphene surfaces. (b) Height profile of the surface along the white dashed line in (a). (c) AFM image of the grating structures on the biomimetic graphene surfaces. (d) Three-dimensional-transformed AFM image of (c). (e) Height profile of the surface along the white dashed line in (c).

large area. The period was  $2\ \mu\text{m}$ . The height profile along the white dashed line in Figure 5a shows that the height of the grating structure ranged from  $500\ \text{nm}$  to  $1.5\ \mu\text{m}$ . To obtain a more accurate value of the average height, the surface was

further characterized by AFM (Figure 5c). The AFM image shows a structure similar to that observed in the SEM image. The 3D-transformed AFM image and height profile along the white dashed line of Figure 5c confirmed the period of the grating ( $2\ \mu\text{m}$ ) and indicated that the height of the grating structure was  $800\text{--}1000\ \text{nm}$  (Figure 5d,e). The height of the grating structure can be tuned by changing the intensity of the laser and the thickness of the GO film.

The two factors that govern the wettability of a solid surface are the surface micro–nanostructures and the surface chemical composition (surface energy). The laser treatment of the GO surface induced the formation of hierarchical micro–nanostructures, which increased the surface roughness and effectively changed the surface chemical composition through a photoreduction process. Therefore, we also investigated the surface chemical composition by X-ray photoelectron spectroscopy (XPS). Figure 6 shows the survey X-ray photoelectron spectra of GO and reduced GO (RGO). The XPS results for GO and RGO show two distinct characteristic peaks at 285 and 533 eV, which correspond to C 1s and O 1s. After the laser treatment, the RGO O 1s peak intensity significantly decreased compared to that of GO, which suggested that GO was effectively reduced into RGO. The C 1s spectra of GO and RGO were deconvoluted into three peaks at 284.6, 286.6, and 288.4 eV, which corresponded to C–C (nonoxygenated ring carbon), C–O (hydroxyl and epoxy carbon), and C=O (carbonyl) (Figure 6b,c). For GO, the oxide atom content was as high as approximately 31.5%, whereas after the laser reduction, the C–O and C=O peaks significantly decreased (Figure 6c). The oxide atom content decreased to 6.8%, which indicated that oxygen-containing functional groups were removed. The XPS results showed that the C–C peak of the structured RGO narrowed compared to that of GO and the C–O peak shifted from 286.6 to 286.0 eV. These changes can be attributed to the effective photoreduction treatment. During this treatment, typical OCGs, such as C–OH (285.6 eV) and C–O–C (286.6 eV), are removed. The removal of these hydrophilic OCGs can significantly change the surface chemical composition, effectively reducing the surface energy. The synergistic effect of the laser-induced micro–nanostructuring and photoreduction creates a superhydrophobic surface. Fourier transform infrared (FT-IR) spectra of GO and RGO (after laser treatment) have been provided as another evidence to prove the deoxygenation of GO (for details, see Supporting Information Figure S10).

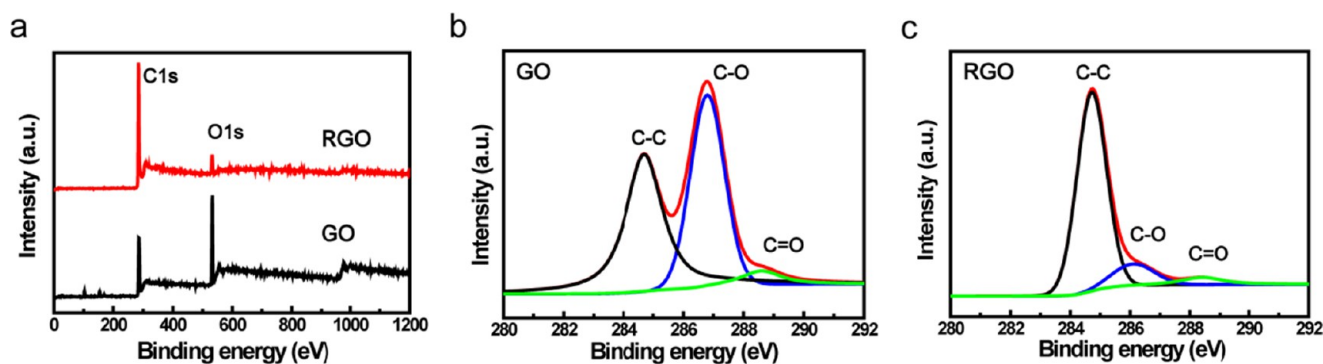


**Figure 6.** (a) Survey X-ray photoelectron spectra of pristine GO and laser-treated RGO surfaces. (b) C 1s XPS images of GO. (c) C 1s XPS images of RGO.

Raman spectroscopy has been considered one of the most reliable and nondestructive methods to characterize graphene and related materials. Figure S2 shows the Raman spectra of GO and laser-treated GO. Notably, the D and G band peaks show neglectable changes after laser treatment. The reason is that the laser cutting and ablation can bring additional new defects on the edges of graphene sheets, which leads to the increase of the D band peak. As a result, the spectra show unobvious changes.

### Wettability of the Biomimetic Graphene Surfaces.

After the surface morphology characterization and chemical component quantitative analysis of the biomimetic graphene surfaces, static water CA and dynamic water SA measurements were used to investigate the wettability along and against the large grooved structure. To specify the hierarchical effect on the superhydrophobicity, we made a full comparison of the dewetting behaviors of flat substrates (SU-8, GO, RGO), groove substrates (SU-8, GO, RGO), grating substrates (RGO), and the hierarchical substrate (RGO, see Supporting Information Figures S1, S4a,b, and Table S1). These results show that the grating structures of RGO account for the superhydrophobicity and the groove structures contribute to the anisotropic dewetting behavior. To investigate the anisotropic wettability, we first analyzed the effect of the large grooved structure on surface wettability. The biomimetic graphene surfaces had grooved structure depths of 50, 100, and 150  $\mu\text{m}$  with a fixed period of 100  $\mu\text{m}$ . Figure 7a shows the CAs along and against the grooved structure. Generally, the periods of the SU-8 grooves were determined by the mask plates. It can be tuned flexibly from tens of nanometers to hundreds of microns. And the depth of the groove structure can

be regulated by the thickness of the SU-8 film. However, to simulate the surface morphology and wettability of real reed leaves, we only choose the 100  $\mu\text{m}$  grooves and adjust the grooves depth to match the periodic size. The CAs varied from 148 to 162 $^\circ$ , which showed the extreme superhydrophobicity of the surfaces. When the groove depth was 100  $\mu\text{m}$ , the CA measured along the grooved structure was 162 $^\circ$ . In contrast, the CA measured from the perpendicular direction slightly decreased to  $\sim$ 157 $^\circ$ . This phenomenon was also observed for the two other grooved surfaces with different depths. The CAs of the sample (groove depth, 10  $\mu\text{m}$ ) measured along the parallel and perpendicular directions were  $\sim$ 100 and 96 $^\circ$ , respectively (Figure S6). By comparing these results, we found that the groove structure with a period of 100  $\mu\text{m}$  (similar to real reed leaves) and a depth of 100  $\mu\text{m}$  is an optimized structure. Further, increase of depth does not show obvious influence on the surface wettability since the droplet cannot wet the bottom of the grooves in this case. The SAs measured along the two directions showed more obvious anisotropy (Figure 7b). When the depth was 50  $\mu\text{m}$ , the SAs measured along and against the groove were 7 and 13 $^\circ$ , respectively. When the groove depth increased to 100  $\mu\text{m}$ , the SA along the parallel direction was 3 $^\circ$ , which was much lower than that measured against the groove direction,  $\sim$ 10 $^\circ$ . An obvious anisotropic superhydrophobicity was observed. Further, increasing the depth to 150  $\mu\text{m}$  did not influence the anisotropic wettability. The biomimetic graphene surface (groove depth of 100  $\mu\text{m}$ ) has exhibited obvious anisotropy in two directions, similar to the natural reed leaf surface.

As previously described, the biomimetic graphene surfaces possess distinct anisotropic dewetting properties due to the presence of hierarchical micro–nanostructures comparable to those on natural reed leaves. However, which structure, i.e., the large grooves or grating structure, is critical to the anisotropic superhydrophobicity is not clear. In controlled experiments, we designed and fabricated a series of biomimetic graphene surfaces with grating structures that were not parallel to the grooves. Instead, the structures formed crossing angles of 45 or 90 $^\circ$ . Generally, the direction of graphene grating structures is parallel to the direction of the light screen and perpendicular to the direction of laser. In this case, to control the angle between the directions of graphene grating and the grooves, we need to make the direction of groove structure parallel to the direction of the light screen first and rotate the substrate at a certain angle (such as 0, 45, and 90 $^\circ$ ) to achieve desired structures. Figure 8 shows the SEM and CLSM images of these biomimetic graphene surfaces, and both the grooves and gratings can be well identified on the grooved surface. In addition to the crossing angle between the grooves and the grating structure, we also changed the depth of the grooves from 50 to 150  $\mu\text{m}$ . To comprehensively compare all of these parameters, we measured the CAs and SAs along and against the grooved structures. The results are summarized in Table 1. Notably, all of these biomimetic graphene surfaces were superhydrophobic, even when the grooves and gratings were in different directions. The depth of the groove structure obviously influences the surface wettability. When the groove depth was 100  $\mu\text{m}$ , which is comparable to the period size, the CAs reached a maximum value. Further, increases in the depth did not affect the wettability. A similar tendency was also observed for the SAs. The SAs decreased with an increase in the depth and reached a constant value at a depth of 100  $\mu\text{m}$ . The influence of the directions of both the grooves and gratings was

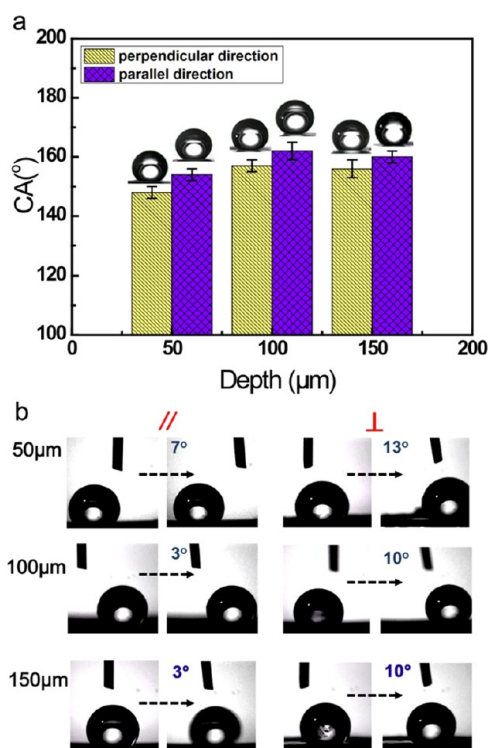


**Figure 7.** (a) Static water CAs of the biomimetic graphene surfaces with different groove depths measured along the directions parallel/perpendicular to the grooves. (b) Dynamic water SAs of the biomimetic graphene surfaces with different groove depths measured along the directions parallel/perpendicular to the grooves.

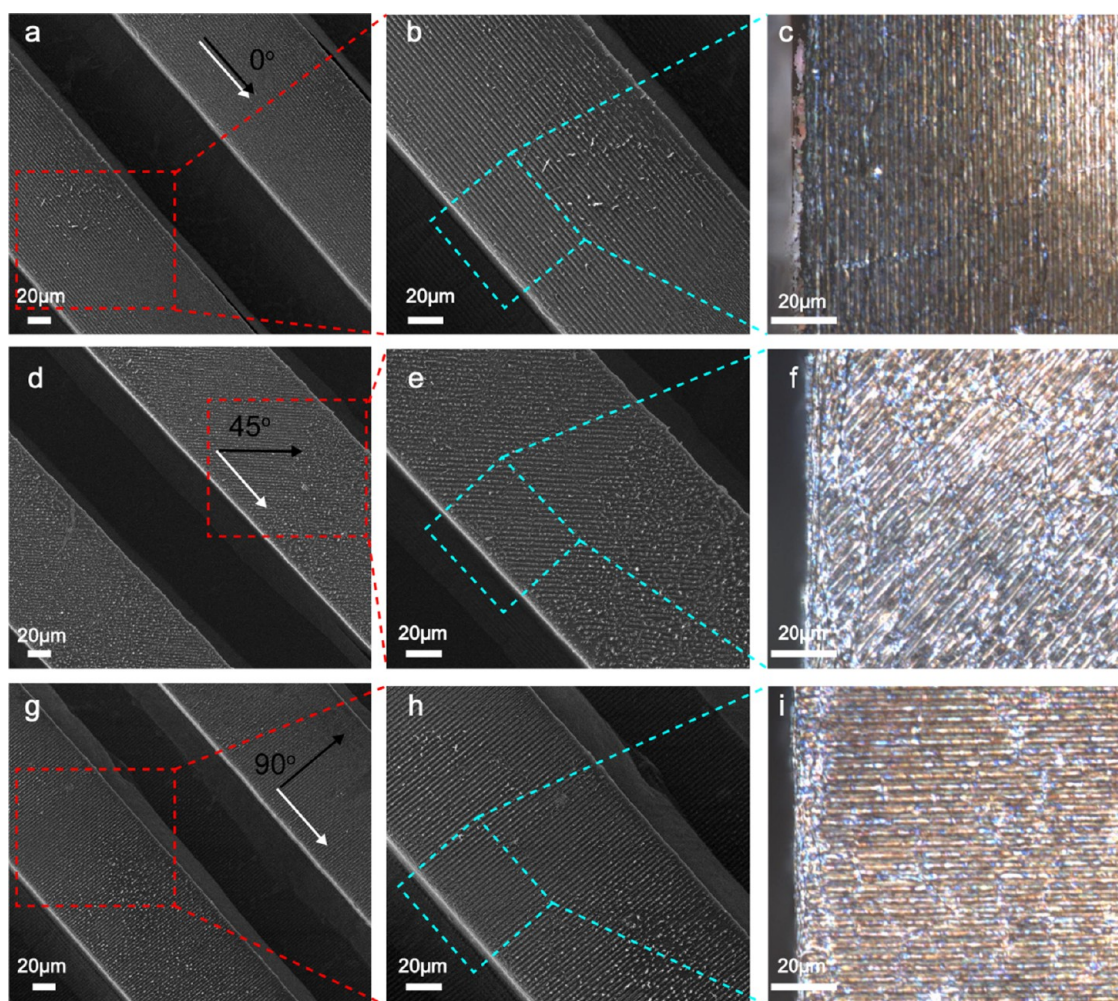


**Figure 8.** (a, b) SEM images and (c) CLSM image of a biomimetic graphene surface with grooves parallel to the grating structure ( $\theta = 0^\circ$ ). (d, e) SEM images and (f) CLSM image of a biomimetic graphene surface with grooves crossing the grating structure ( $\theta = 45^\circ$ ). (g, h) SEM images and (i) CLSM image of a biomimetic graphene surface with groove perpendicular to the grating structure ( $\theta = 90^\circ$ ).

**Table 1. Anisotropic Wettability (CAs and SAs) of the Different Biomimetic Graphene Surfaces**

$\theta$ (deg) <sup>a</sup>	depth: 50 $\mu\text{m}$		depth: 100 $\mu\text{m}$		depth: 150 $\mu\text{m}$	
	CA/SA (deg) <sup>b</sup>	CA/SA (deg) <sup>c</sup>	CA/SA (deg) <sup>b</sup>	CA/SA (deg) <sup>c</sup>	CA/SA (deg) <sup>b</sup>	CA/SA (deg) <sup>c</sup>
0	$154 \pm 2/7 \pm 1$	$148 \pm 2/13 \pm 1$	$162 \pm 2/3 \pm 1$	$157 \pm 3/10 \pm 2$	$162 \pm 3/3 \pm 1$	$157 \pm 2/10 \pm 2$
45	$152 \pm 3/8 \pm 2$	$145 \pm 2/12 \pm 2$	$160 \pm 3/5 \pm 2$	$155 \pm 2/10 \pm 3$	$160 \pm 2/6 \pm 2$	$154 \pm 3/10 \pm 3$
90	$150 \pm 3/10 \pm 2$	$142 \pm 3/13 \pm 2$	$157 \pm 2/5 \pm 2$	$153 \pm 2/11 \pm 2$	$156 \pm 3/5 \pm 1$	$153 \pm 2/12 \pm 1$

<sup>a</sup>The cross angle between the grating and groove directions. <sup>b</sup>CA and SA measured from the direction parallel to the groove. <sup>c</sup>CA and SA measured from the direction perpendicular to the groove.

also evaluated. When the grating was parallel to the grooves, the surfaces had larger CAs than those with cross-angle gratings and grooves. The CAs observed from two directions gradually decreased with an increase in the cross angle. These results indicated that natural reed leaves possess optimized hierarchical structures with small microstructures that are parallel to the grooves. Finally, the grooves play a critical role in the anisotropic wettability. The droplet sliding performance measurements showed that the SAs measured along the grooves were much smaller than those measured along the grating structures (against the groove when the cross angle was  $90^\circ$ ).

## CONCLUSIONS

Inspired by natural reed leaf surfaces that demonstrate anisotropic wettability along both directions of the leaf vein, we developed an ingenious method to produce biomimetic graphene surfaces using a combination of photolithography and laser holography technologies. Grooved substrates with a period of 200  $\mu\text{m}$  were fabricated by photolithography using photopolymers. After coating the substrates with a layer of GO, a two-beam laser interference treatment was performed to induce additional grating-like micro-nanostructures. The as-formed hierarchical micro-nanostructures endowed the graphene film with anisotropic wettability similar to that of reed leaves. The laser treatment triggered the formation of rough micro-nanostructures and altered the surface energy by

removing hydrophilic groups. We systematically investigated the influence of the groove depth and orientation of the groove/grating structures on the anisotropic wettability and discovered that the grooved structure, not the grating structure, governed the droplet sliding behavior. Inspired from the anisotropic superhydrophobicity of reed leaves, solid surfaces with similar dewetting properties have found broad applications in both fundamental science and industrial usage.<sup>37–40</sup> In this study, we successfully impart the reed leaf-inspired wettability to graphene surfaces by constructing hierarchical structures. The combination of anisotropic superhydrophobicity with graphene surfaces would undoubtedly motivate various cutting-edge applications, such as biochips enabling flexible droplet manipulation, bionic electronics with waterproof coating, and biocompatible substrates for tissue engineering.

## ■ ASSOCIATED CONTENT

### Supporting Information

The Supporting Information is available free of charge on the ACS Publications website at DOI: [10.1021/acsami.8b03738](https://doi.org/10.1021/acsami.8b03738).

Wettability of micrograting graphene surface and the hierarchical graphene surface; Raman spectra of GO and RGO; AFM image for the GO thickness; wettability of GO and RGO surfaces; SEM image of hierarchical graphene surface on grooved PDMS substrate; wettability of the biomimetic graphene surfaces with different groove depths; photograph of the biomimetic graphene surface spot; CLSM images of flat GO; wettability of SU-8 groove surface before and after O<sub>2</sub> plasma treatment; FT-IR spectra of GO and RGO; and wettability tests of different substrates (Table S1) (PDF)

## ■ AUTHOR INFORMATION

### Corresponding Authors

\*E-mail: [yonglaizhang@jlu.edu.cn](mailto:yonglaizhang@jlu.edu.cn) (Y.-L.Z.).

\*E-mail: [hbsun@tsinghua.edu.cn](mailto:hbsun@tsinghua.edu.cn) (H.-B.S.).

### ORCID

Yong-Lai Zhang: [0000-0002-4282-250X](https://orcid.org/0000-0002-4282-250X)

### Author Contributions

The manuscript was written through contributions of all authors. All authors have given approval to the final version of the manuscript.

### Notes

The authors declare no competing financial interest.

## ■ ACKNOWLEDGMENTS

This study was supported by the National Key Research and Development Program of China and National Natural Science Foundation of China (NSFC) under Grants #2017YFB1104300, #61522503, #61775078, #61590930, and #51705192. The project was funded by the China Postdoctoral Science Foundation, 2017M611325, and the National Postdoctoral Program for Innovative Talents, BX201600064.

## ■ REFERENCES

- (1) Liu, K. S.; Jiang, L. Multifunctional Integration: From Biological to Bio-Inspired Materials. *ACS Nano* **2011**, *5*, 6786–6790.
- (2) Sanchez, C.; Arribart, H.; Guille, M. M. G. Biomimeticism and bioinspiration as tools for the design of innovative materials and systems. *Nat. Mater.* **2005**, *4*, 277–288.

- (3) Meyers, M. A.; Chen, P. Y.; Lin, A. Y. M.; Seki, Y. Biological materials: Structure and mechanical properties. *Prog. Mater. Sci.* **2008**, *53*, 1–206.

- (4) Chen, Y.; Zang, X. N.; Gu, J. J.; Zhu, S. M.; Su, H. L.; Zhang, D.; Hu, X. B.; Liu, Q. L.; Zhang, W.; Liu, D. X. ZnO single butterfly wing scales: synthesis and spatial optical anisotropy. *J. Mater. Chem.* **2011**, *21*, 6140–6143.

- (5) Kinoshita, S.; Yoshioka, S. Structural colors in nature: The role of regularity and irregularity in the structure. *ChemPhysChem* **2005**, *6*, 1442–1459.

- (6) Park, J. T.; Kim, J. H.; Lee, D. Excellent anti-fogging dye-sensitized solar cells based on superhydrophilic nanoparticle coatings. *Nanoscale* **2014**, *6*, 7362–7368.

- (7) Wu, D.; Wu, S. Z.; Chen, Q. D.; Zhang, Y. L.; Yao, J.; Yao, X.; Niu, L. G.; Wang, J. N.; Jiang, L.; Sun, H. B. Curvature-Driven Reversible In Situ Switching Between Pinned and Roll-Down Superhydrophobic States for Water Droplet Transportation. *Adv. Mater.* **2011**, *23*, 545–549.

- (8) Wu, D.; Wang, J. N.; Niu, L. G.; Zhang, X. L.; Wu, S. Z.; Chen, Q. D.; Lee, L. P.; Sun, H. B. Bioinspired Fabrication of High-Quality 3D Artificial Compound Eyes by Voxel-Modulation Femtosecond Laser Writing for Distortion-Free Wide-Field-of-View Imaging. *Adv. Opt. Mater.* **2014**, *2*, 751–758.

- (9) Fan, L.; Li, B. C.; Zhang, J. P. Antibioadhesive Superhydrophobic Syringe Needles Inspired by Mussels and Lotus Leaves. *Adv. Mater. Interfaces* **2015**, *2*, No. 1500019.

- (10) Feng, L.; Zhang, Y. A.; Cao, Y. Z.; Ye, X. X.; Jiang, L. The effect of surface microstructures and surface compositions on the wettabilities of flower petals. *Soft Matter* **2011**, *7*, 2977–2980.

- (11) Chen, H.; Zhang, P. F.; Zhang, L. W.; Iu, H. L. L.; Jiang, Y.; Zhang, D. Y.; Han, Z. W.; Jiang, L. Continuous directional water transport on the peristome surface of *Nepenthes alata*. *Nature* **2016**, *532*, 85–89.

- (12) Feng, L.; Li, S. H.; Li, Y. S.; Li, H. J.; Zhang, L. J.; Zhai, J.; Song, Y. L.; Liu, B. Q.; Jiang, L.; Zhu, D. B. Super-hydrophobic surfaces: From natural to artificial. *Adv. Mater.* **2002**, *14*, 1857–1860.

- (13) Wang, B.; Guo, Z. G. Superhydrophobic copper mesh films with rapid oil/water separation properties by electrochemical deposition inspired from butterfly wing. *Appl. Phys. Lett.* **2013**, *103*, 5.

- (14) Zhang, Z.; Huang, J. D.; Dong, B.; Yuan, Q.; He, Y. Y.; Wolfbeis, O. S. Rational tailoring of ZnSnO<sub>3</sub>/TiO<sub>2</sub> heterojunctions with bioinspired surface wettability for high-performance humidity nano-sensors. *Nanoscale* **2015**, *7*, 4149–4155.

- (15) Liu, K. S.; Tian, Y.; Jiang, L. Bio-inspired superoleophobic and smart materials: Design, fabrication, and application. *Prog. Mater. Sci.* **2013**, *58*, 503–564.

- (16) Wang, J. N.; Shao, R. Q.; Zhang, Y. L.; Guo, L.; Jiang, H. B.; Lu, D. X.; Sun, H. B. Biomimetic Graphene Surfaces with Superhydrophobicity and Iridescence. *Chem. - Asian J.* **2012**, *7*, 301–304.

- (17) Sun, Y. L.; Dong, W. F.; Yang, R. Z.; Meng, X.; Zhang, L.; Chen, Q. D.; Sun, H. B. Dynamically Tunable Protein Microlenses. *Angew. Chem., Int. Ed.* **2012**, *51*, 1558–1562.

- (18) Zheng, Z. B.; Li, J. T.; Ma, T.; Fang, H. L.; Ren, W. C.; Chen, J.; She, J. C.; Zhang, Y.; Liu, F.; Chen, H. J.; Deng, S. Z.; Xu, N. S. Tailoring of electromagnetic field localizations by two-dimensional graphene nanostructures. *Light: Sci. Appl.* **2017**, *6*, No. e17057.

- (19) Rodrigo, D.; Tittel, A.; Limaj, O.; de Abajo, F. J. G.; Pruneri, V.; Altug, H. Double-layer graphene for enhanced tunable infrared plasmonics. *Light: Sci. Appl.* **2017**, *6*, No. e16277.

- (20) Morozov, S. V.; Novoselov, K. S.; Katsnelson, M. I.; Schedin, F.; Elias, D. C.; Jaszczak, J. A.; Geim, A. K. Giant intrinsic carrier mobilities in graphene and its bilayer. *Phys. Rev. Lett.* **2008**, *100*, No. 016602.

- (21) Xu, Z.; Liu, Z.; Sun, H. Y.; Gao, C. Highly Electrically Conductive Ag-Doped Graphene Fibers as Stretchable Conductors. *Adv. Mater.* **2013**, *25*, 3249–3253.

- (22) Li, X.; Zhu, Y. W.; Cai, W. W.; Borysiak, M.; Han, B. Y.; Chen, D.; Piner, R. D.; Colombo, L.; Ruoff, R. S. Transfer of Large-Area

Graphene Films for High-Performance Transparent Conductive Electrodes. *Nano Lett.* **2009**, *9*, 4359–4363.

(23) Qian, Z. S.; Shan, X. Y.; Chai, L. J.; Ma, J. J.; Chen, J. R.; Feng, H. A universal fluorescence sensing strategy based on biocompatible graphene quantum dots and graphene oxide for the detection of DNA. *Nanoscale* **2014**, *6*, 5671–5674.

(24) Sealy, C. Making high-speed graphene transistors with nanowires. *Nano Today* **2010**, *5*, 509–510.

(25) Zhang, X. Y.; Sun, S. H.; Sun, X. J.; Zhao, Y. R.; Chen, L.; Yang, Y.; Lu, W.; Li, D. B. Plasma-induced, nitrogen-doped graphene-based aerogels for high-performance supercapacitors. *Light: Sci. Appl.* **2016**, *5*, No. e16130.

(26) Park, H.; Brown, P. R.; Buloyic, V.; Kong, J. Graphene As Transparent Conducting Electrodes in Organic Photovoltaics: Studies in Graphene Morphology, Hole Transporting Layers, and Counter Electrodes. *Nano Lett.* **2012**, *12*, 133–140.

(27) Zhang, Y. L.; Chen, Q. D.; Jin, Z.; Kim, E.; Sun, H. B. Biomimetic graphene films and their properties. *Nanoscale* **2012**, *4*, 4858–4869.

(28) Han, D. D.; Zhang, Y. L.; Ma, J. N.; Liu, Y. Q.; Han, B.; Sun, H. B. Light-Mediated Manufacture and Manipulation of Actuators. *Adv. Mater.* **2016**, *28*, 8328–8343.

(29) Yong, J.; Chen, F.; Yang, Q.; Hou, X. Femtosecond laser controlled wettability of solid surfaces. *Soft Matter* **2015**, *11*, 8897–8906.

(30) Zang, J.; Ryu, S.; Pugno, N.; Wang, Q. M.; Tu, Q.; Buehler, M. J.; Zhao, X. H. Multifunctionality and control of the crumpling and unfolding of large-area graphene. *Nat. Mater.* **2013**, *12*, 321–325.

(31) Singh, E.; Chen, Z. P.; Houshmand, F.; Ren, W. C.; Peles, Y.; Cheng, H. M.; Koratkar, N. Superhydrophobic Graphene Foams. *Small* **2013**, *9*, 75–80.

(32) Chen, Z.; Li, H.; Tian, R.; Duan, H. A.; Guo, Y. P.; Chen, Y. J.; Zhou, J.; Zhang, C. M.; Dugnani, R.; Liu, H. Z. Three dimensional Graphene aerogels as binder-less, freestanding, elastic and high-performance electrodes for lithium-ion batteries. *Sci. Rep.* **2016**, *6*, No. 27365.

(33) Jiang, H. B.; Zhang, Y. L.; Han, D. D.; Xia, H.; Feng, J.; Chen, Q. D.; Hong, Z. R.; Sun, H. B. Bioinspired Fabrication of Superhydrophobic Graphene Films by Two-Beam Laser Interference. *Adv. Funct. Mater.* **2014**, *24*, 4595–4602.

(34) Xue, Y.; Liu, Y.; Lu, F.; Qu, J.; Chen, H.; Dai, L. M. Functionalization of Graphene Oxide with Polyhedral Oligomeric Silsesquioxane (POSS) for Multifunctional Applications. *J. Phys. Chem. Lett.* **2012**, *3*, 1607–1612.

(35) Rafiee, J.; Rafiee, M. A.; Yu, Z. Z.; Koratkar, N. Superhydrophobic to Superhydrophilic Wetting Control in Graphene Films. *Adv. Mater.* **2010**, *22*, 2151–2154.

(36) Lin, Y.; Ehlert, G. J.; Bukowsky, C.; Sodano, H. A. Superhydrophobic Functionalized Graphene Aerogels. *ACS Appl. Mater. Interfaces* **2011**, *3*, 2200–2203.

(37) Wang, Z.; Elimelech, M.; Lin, S. Environmental Applications of Interfacial Materials with Special Wettability. *Environ. Sci. Technol.* **2016**, *50*, 2132–2150.

(38) Li, S.; Huang, J.; Chen, Z.; Chen, G.; Lai, Y. A review on special wettability textiles: theoretical models, fabrication technologies and multifunctional applications. *J. Mater. Chem. A* **2017**, *5*, 31–55.

(39) Jiaqiang, E.; Jin, Y.; Deng, Y.; Zuo, W.; Zhao, X.; Han, D.; Peng, Q.; Zhang, Z. Wetting Models and Working Mechanisms of Typical Surfaces Existing in Nature and Their Application on Superhydrophobic Surfaces: A Review. *Adv. Mater. Interfaces* **2018**, *5*, No. 1701052.

(40) Bhushan, B. Biomimetics: lessons from nature—an overview. *Philos. Trans. R. Soc., A* **2009**, *367*, 1445–1486.